Spin-phonon coupling in the incommensurate magnetic ordered phase of orthorhombic TmMnO3

Spin-phonon coupling in Incommensurate magnetic ordered phase of orthorhombic $TmMnO_3$

B. S. Araújo[1,2], A. M. Arevalo-Lopez[2,3], C. C. Santos[4], J. P. Attfield[2], C. W. A. Paschoal[1], A. P. Ayala[1]

[1] Physics Department, Universidade Federal do Ceará, PO Box 6030, Campus do Pici, 60455-760 Fortaleza - CE, Brazil
[2] Centre for Science at Extreme Conditions (CSEC) and School of Chemistry, The University of Edinburgh, Peter Guthrie Tait Road, Edinburgh EH9 3FD, United Kingdom.
[3]University of Lille, CNRS, Centrale Lille, ENSCL, University Artois, UMR 8181 - UCCS - Unité de Catalyse et Chimie du Solide, F-59000 Lille, France
[4] Physics Department, CCET, Universidade Federal do Maranhão, PO Box 65085-580 São Luís – MA, Brazil

ABSTRACT

The search for materials with strong magnetoelectric coupling has been intense since interesting properties were discovered in the perovskite $TbMnO_3$,. Among the manganese-based perovskite family ($RMnO_3$), magnetic and electric orders coexist in the orthorhombic phase of the distorted perovskite $TmMnO_3$. The antiferromagnetic phase induces ferroelectricity, leading to type–II multiferroic behaviour. Although the temperature-dependent behavior of the Raman-active phonons of other members of the orthorhombic $RMnO_3$ family was already reported, little information about orthorhombic $TmMnO_3$ is published. In this paper, we report the temperature-dependent Raman spectra of bulk orthorhombic $TmMnO_3$. A weak spin-phonon coupling was observed in the incommensurate antiferromagnetic ordered phase around 44 K. Raman spectra are also sensitive to the magnetic transition from the incommensurate to E-type antiferromagnetic phase, where no spin-phonon coupling is detected. The possibility of an orbital-spin-phonon coupling was investigated and described based on the magnetic ordering of the low-temperature phase.

1. Introduction

Orthorhombic manganite perovskites $RMnO_3$ (o-RMO) have been extensively investigated because of their exciting properties such as charge ordering, magnetoresistance, and multiferroicity (Baldini et al., 2018; Goto et al., 2004; Hwang et al., 1995; Kenzelmann et al., 2005; Kimura, Goto, et al., 2003; Spaldin & Ramesh, 2019). At ambient conditions, large R^{3+} ionic radii (r_R) lead the $RMnO_3$ perovskites to assume

an orthorhombic structure presenting an A-type antiferromagnetic (AFM) ordered phase (Goto et al., 2004; Kimura, Ishihara, et al., 2003). Whereas, in the case of smaller r_R, an hexagonal structure is preferred (Martín-Carrón et al., 2001; Salama et al., 2010; Zhou et al., 2006), and their magnetic order is E-type AFM or an incommensurate structure (Goto et al., 2004; Kimura, Ishihara, et al., 2003). However, in compounds with small r_R, the orthorhombic phase can also be stabilized by High-Pressure and High-Temperature (HP/HT) treatments (Uusi-Esko et al., 2008).

Belonging to the group of small r_R, $TmMnO_3$ (TMO) crystallizes in a hexagonal structure with a *P6₃cm* space group. This structure can be described as layers of bipyramids of MnO_5 separated by layers of Tm^{3+} (Uusi-Esko et al., 2008). Wang et al. (Wang et al., 2007) studied the ferroelectric behavior of hexagonal $TmMnO_3$ *(h*-TMO), reporting a ferro-paraelectric phase transition around 621 K, while Yen et al. (Yen et al., 2007) observed a magnetic transition around 84 K. Later, Massa et al. (Massa et al., 2014) confirmed the electric and magnetic transitions showing a ferroelectric-magnetic coupling in the magnetically ordered phase using far-infrared emissivity and reflectivity spectra analysis.

The orthorhombic phase of $TmMnO_3$ (*o*-TMO), which is stabilized through HP/HT treatment, belongs to the *Pbnm* space group. This structure can be described as a distorted perovskite with corner-sharing MnO_6 octahedra in a tridimensional network and Tm^{3+} ions located at the free space between these octahedra. Using specific heat measurements, Tachibana et al. (Tachibana et al., 2007) reported a magnetic transition in *o*-TMO around 43 K. Later, Pomjakushin (Mukherjee et al., 2017; Pomjakushin et al., 2009) classified the magnetic structure of *o*-TMO as incommensurate below 43 K observing a second magnetic transition at 32 K, where the incommensurate structure become an E-type AFM. In the same study, the authors reported dielectric susceptibilities and pyroelectric measurements showing the existence of a spontaneous electric polarization appearing below 32 K, originated by lattice distortions due to the E-type AFM phase. These features evidence a multiferroic phase in *o*-TMO for bulk samples. Such multiferroic behavior was also confirmed by Salama et al. (Salama et al., 2010) using Mössbauer spectroscopy, while Han et al. (Han & Chao, 2010) observed this phase in thin films. Moreover, these observations were confirmed through resonant X-ray analysis in bulk samples by Garganourakis *et al*. (Garganourakis et al., 2012) and in thin films by Windsor et al. (Windsor et al., 2015)

Recently, Shimamoto et al. (Shimamoto et al., 2017) reported the room temperature Raman spectra of the orthorhombic $RMnO_3$ (R = Gd - Lu) family (*o*-RMO) obtained as thin films on a $YAlO_3$ substrate. This study evidences that the chemical pressure influence along the *b*-axis, since the R^{3+} ion change induces a shift of oxygen atoms on the *ac* plane, increasing the wavenumber of some vibrational modes in comparison to the values reported for bulk samples. Even though the Raman spectrum of *o*-TMO on a thin film was presented, there is neither information about the vibrational spectrum of bulk *o*-TMO nor its temperature dependence.

The spin-phonon coupling in the *o*-RMO family was reported by Granado et al. (Granado et al., 1999) and Laverdière et al. (Laverdière et al., 2006), where the latter authors affirm the coupling effect in small r_R compounds and incommensurate AFM is negligible, whereas in E-type AFM ordered compounds, the coupling effect should be very weak or absent (Laverdière et al., 2006).

In the case of TMO, the spin-phonon coupling was confirmed in the hexagonal phase using far-infrared spectroscopy (Basistyy et al., 2014). In this study, the authors observed a phonon renormalization occurring at the magnetically ordered phase for *h*-TMO, where the renormalization effects were estimated to be around 5 cm^{-1}.

The coupling between electric and magnetic ordering observed in *h*-TMO suggests that the magnetic ordering can also couple with the lattice phonons in case of *o*-TMO. Due to its sensibility to detect magnetic orderings through the coupling with the phonon lattice, mainly in perovskites compounds (Niitaka et al., 2004; Sugawara et al., 1965, 1968), Raman spectroscopy was employed to investigate the multiferroic properties of *o*-TMO by monitoring the spin-phonon coupling effect through its low-temperature magnetic transitions.

2. Experimental Session

Polycrystalline o-TMO samples were obtained through an HP/HT treatment of *h*-TMO. *h*-TMO polycrystalline samples were synthesized by solid-state reaction. Stoichiometric amounts of Tm_2O_3 (REacton, 99.99%) and Mn_2O_3 (Aldrich, 99.99%) were grounded together in an agate mortar, and the mixture was calcined in a conventional oven at 1200 °C during 24 hours. In sequence, *h*-TMO pellets were grounded and sealed into platinum capsules and treated at 1573 K under 6 GPa during 60 min in a Walker type multianvil press. After the reaction, the system was quenched to room temperature (RT), and the pressure was slowly released until atmospheric pressure. The resultant dark-green

dense pellets were characterized by X-ray diffraction (XRD) on a BRUKER D8 diffractometer (Cu $K\alpha_1$ radiation 1.5406 Å) to confirm the stabilization of orthorhombic phase.

Raman spectroscopy measurements were performed in a Jobin-Yvon T64000 Triple Spectrometer configured in a backscattered geometry. The 633 nm line of a HeNe gas laser operating at 20 mW, focused on the sample by a long-working distance objective (20x, 20.5 mm), was used to excite the signal that was collected in an N_2-cooled CCD system. The spectrometer slits were configured to obtain a spectra resolution lower than 1 cm^{-1}. Temperature-dependent Raman measurements from 10 up to 300 K were carried out by using a closed-cycle He cryostat in which the temperature was controlled by a Lakeshore temperature controller model 330S with a precision of 0.1 K. The Raman spectra were deconvoluted with Lorentzian functions using the Fityk software (Wojdyr, 2010)

3. Results

The as-synthesized $TmMnO_3$, obtained by solid-state reaction, presented the $P6_3cm$ space group with lattice parameters $a = 6.09270$ Å and $c = 11.39080$ Å. Through an HP/HT treatment, the crystalline structure of the hexagonal TMO phase was converted into orthorhombic *Pbnm*. The X-ray Rietveld refinement results for the orthorhombic phase presented the lattice parameters a= 5.232(x) Å, b= 5.814(x) Å, and c= 7.324(x) Å, in good agreement with the literature (Uusi-Esko et al., 2008). This phase is identified as an orthorhombically distorted-perovskite structure where the Mn^{3+} ions are octahedrally coordinated with six oxygen ions forming a distorted corner-sharing MnO_6 network, whereas Tm^{3+} ions are located at the free space between those octahedra (inset of figure 1).

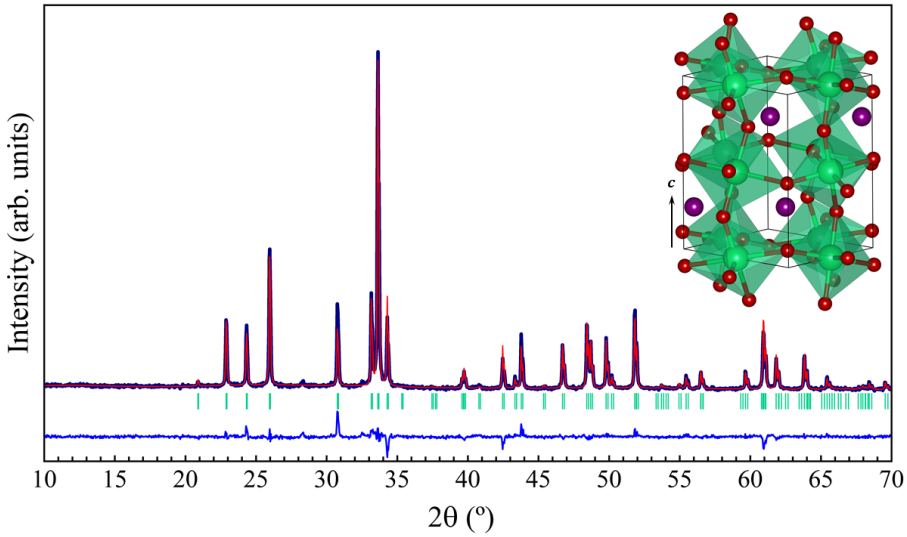

Figure 1. Powder XRD pattern and Rietveld refinement of the *o*-TMO sample. The green bars indicate the reflection positions of *o*-TMO(Uusi-Esko et al., 2008) (ICSD card number 162209).

The room temperature Raman spectrum of *o*-TMO is shown in Figure 2. Based on group theory analysis, the distribution of Raman-active irreducible representations of the D_{2h} factor group at the Γ point of Brillouin zone is $7A_g \oplus 5B_{1g} \oplus 7B_{2g} \oplus 5B_{3g}$ (Bauman et al., 1981). Based on this analysis, 24 modes of mixed symmetries are predicted in the Raman spectra of the o-$TmMnO_3$ polycrystalline sample. In our Raman analysis, we were able to identify 13 vibrational modes, the most intense one being located around 620 cm^{-1}.

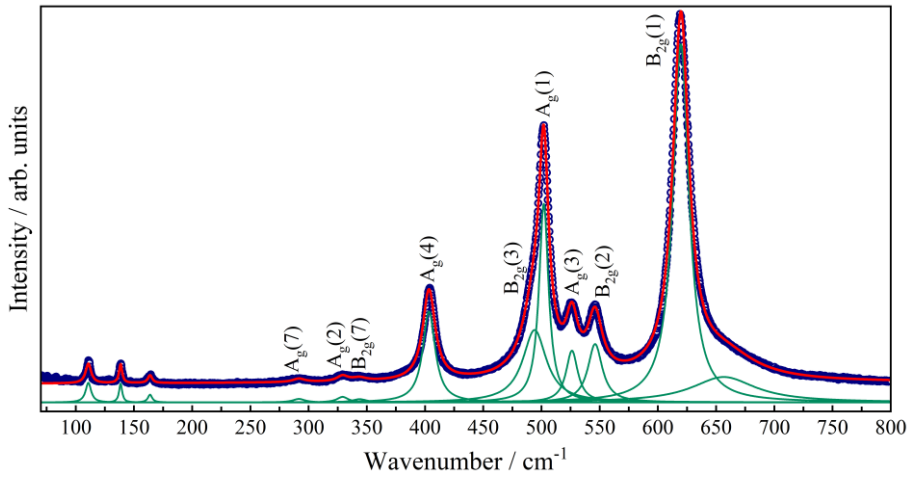

Figure 2. Orthorhombic $TmMnO_3$ Raman spectrum at room temperature.

The assignments of the observed Raman modes can be made based on other *o*-RMO compounds (de Andrés et al., 1999; Iliev et al., 2006; Martín-Carrón et al., 2001, 2002). In such studies, the authors have shown that the MnO_6 phonon positions depend

on the R^{3+} ionic radius (r_R). Iliev et al. (Iliev et al., 2006) reported a theoretical dynamic calculation model for the r_R dependence of the phonon energy for the most intense $A_g(3)$, $A_g(1)$ and $B_{2g}(1)$ bands, showing that the decrease on r_R implies that the $A_g(3)$ frequency should be higher than the one of $A_g(1)$, while the $B_{2g}(1)$ mode should be the most intense one.

In the case of *o*-TMO, the external modes are located below 200 cm^{-1}, while those modes with higher wavenumbers are related to MnO_6 octahedron internal modes (Table 1). The three very weak modes observed at 290, 329, and 343 cm^{-1} have $A_g(7)$, $A_g(2)$, and $B_{2g}(7)$ symmetries, respectively. The $A_g(7)$ and $B_{2g}(7)$ modes are related to the basal octahedron oxygen motions along x and z directions, while the $A_g(2)$ mode can be related to in-phase MnO_6 rotations around the y-axis. The modes located around 404 and 493 cm^{-1} present symmetries $A_g(4)$ and $B_{2g}(3)$ assigned as out-of-phase MnO_6 rotations along x-axis and bendings, respectively. At higher wavenumbers, the mode located at 502 cm^{-1} originates from oxygen stretching having $A_g(1)$ symmetry, while the one located at 526 cm^{-1} has $A_g(3)$ symmetry being related to MnO_6 octahedra bending. Finally, the modes at 546 and 619 cm^{-1} have B_{2g} symmetry and are assigned to in-phase O_2 "scissors-like" and stretching motions, respectively.

Table 1. Assignment of active Raman modes observed for o-$TmMnO_3$

Frequency (cm^{-1})	Assignment	Motion
290	$A_g(7)$	O_1 (x)
329	$A_g(2)$	In-phase MnO_6 *y* rotations
343	$B_{2g}(7)$	O_1 (z)
404	$A_g(4)$	Out-of-phase MnO_6 *x* rotations
493	$B_{2g}(3)$	Out-of-phase MnO_6 bending
502	$A_g(1)$	O_2 antistretching
526	$A_g(3)$	MnO_6 bending
546	$B_{2g}(2)$	In-phase O_2 "scissors-like"
619	$B_{2g}(1)$	In-plane O_2 stretching

The only prior Raman study of *o*-TMO was recently reported by Shimamoto et al. (Shimamoto et al., 2017), where they analyze the Raman spectra of *o*-TMO thin films. In this study, the authors were able to investigate only the A_g modes and their respective

positions are very close to those observed here. As stated, the subtle divergences in the phonon energies are given by the epitaxial film strain, which shifts the Raman modes to higher wavenumbers when compared to bulk samples.

The *o*-TMO temperature-dependent Raman measurements were carried out in the temperature range between 300 and 15 K. In view of resolution limitations, the temperature dependence of three A_g and three B_g modes with mixed symmetries (Figure 3) were analyzed, while the modes observed between 280 and 360 cm^{-1} were too weak to be monitored. During the cooling process, the Raman spectra did not present any remarkable change in terms of additional or suppressed bands. Only the usual high-frequency shift and the sharpening of vibrational modes were observed. Therefore, the overall signature of Raman spectra is maintained within the investigated temperature range, implying that the orthorhombic phase of $TmMnO_3$ did not undergo a structural phase transition at low temperatures.

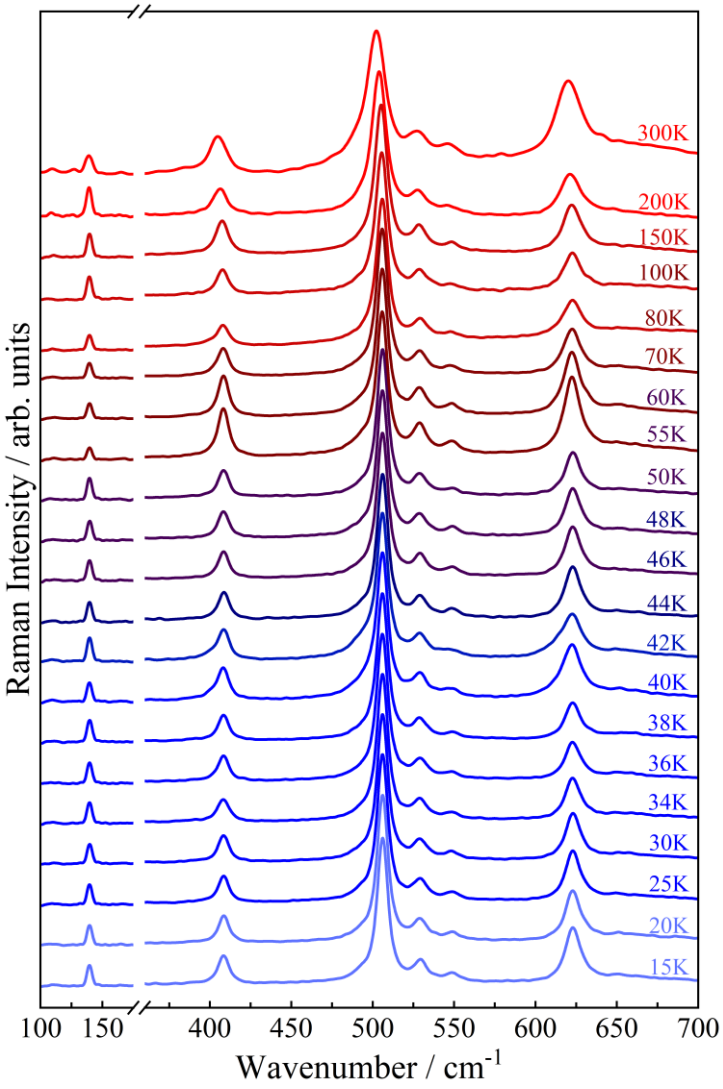

Figure 3. Temperature-dependent Raman spectra of *o*-TMO.

In the absence of significant structural changes, the temperature-dependent behavior of a phonon of frequency ω is mainly governed by the phonon anharmonicity hardening. This behavior was described by Balkanski et al. (Balkanski et al., 1983) using a model that takes into account up to three phonon interactions. The temperature dependence of the wavenumber ($\omega(T)$) and full width at half maximum ($\Gamma(T)$) are given by equations (1) and (2), respectively.

$$\omega(T) = \omega_0 + A\left[1 + \frac{2}{(e^x - 1)}\right] + B\left[1 + \frac{3}{(e^y - 1)} + \frac{3}{(e^y - 1)^2}\right] \quad (1)$$

$$\Gamma(T) = C\left[1 + \frac{2}{(e^x - 1)}\right] + D\left[1 + \frac{3}{(e^y - 1)} + \frac{3}{(e^y - 1)^2}\right] \quad (2)$$

where ω_0, A, B, C, and D are fitting parameters. The terms x and y are $\hbar\omega_0/2K_BT$ and $\hbar\omega_0/3K_BT$, respectively.

Figure 4 shows the temperature dependence of selected phonon wavenumbers and full width at half maximum (FWHM) compared to the Balkanski's model. The phonon wavenumbers follow very well the anharmonic model down to 44 K, where a clear departure from the theoretical curve is observed. At this temperature, a magnetic transition has been reported from a paramagnetic to an incommensurate AFM phase. Thus, the sudden frequency hardening of these vibrational modes starts around the temperature at which the spin moments become aligned is a clear indication of a spin-phonon coupling effect in *o*-TMO.

It is important to note that Pomjakushin and co-workers (Pomjakushin et al., 2009) reported that o-TMO experiences a coupling effect between the lattice parameters and the magnetic ordering below T_N, showing the existence of a lattice distortion stronger than those observed in others members of the o-RMO family. Based on this feature, the renormalization effects on phonon positions observed here could also be induced by the lattice distortions instead of a spin-phonon coupling. Once FWHM is related to the phonon lifetime (Eiter et al., 2014), the effects directly connected to lattice variations do not influence this parameter, allowing us to distinguish phenomena generated by the spin-lattice coupling from those originated in other kinds of coupling effects, such as the spin-phonon. Thus, the study of the phonon FWHM becomes crucial to solve the ambiguity related to the origin of the frequency renormalization. The temperature dependence of the FWHM of selected phonons is also presented in Figure 4, where departures from the anharmonic model can also be noticed around 45 K, suggesting that spin-phonon coupling originates the observed effects.

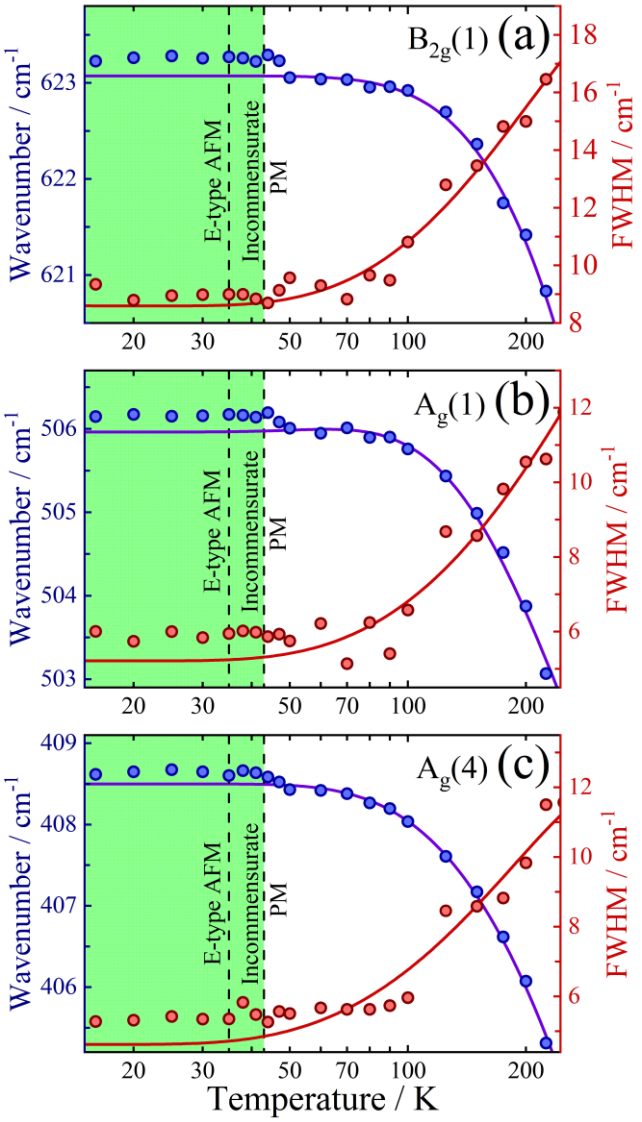

Figure 4. Temperature dependence of selected phonon wavenumber and FWHM of orthorhombic $TmMnO_3$. Solid lines in purple and red indicate the fit based on Balkanski's model for phonons positions and FWHM, respectively. The dashed lines locate the magnetic transitions reported in the literature.

Additional evidence in favor of the spin-phonon origin of the phonon renormalization can be given by considering lattice distortions. The phonon frequency shift induced by changes in ionic binding energies due to lattice distortions can be approximated based on the Grüneisen law: $\delta\omega_\alpha(T) = -\gamma_\alpha\omega_0(\Delta V/V_0)$, where γ_α is the Grüneisen parameter for the normal mode α. Thus, if the phonon energy change is due to lattice distortions, it could be expected to be correlated with the directions or planes (A) closely related to the atomic displacements of a given phonon: $\delta\omega_\alpha(T) = -\gamma_\alpha\omega_0(\Delta A/A_0)$ (Mansouri et al., 2017).

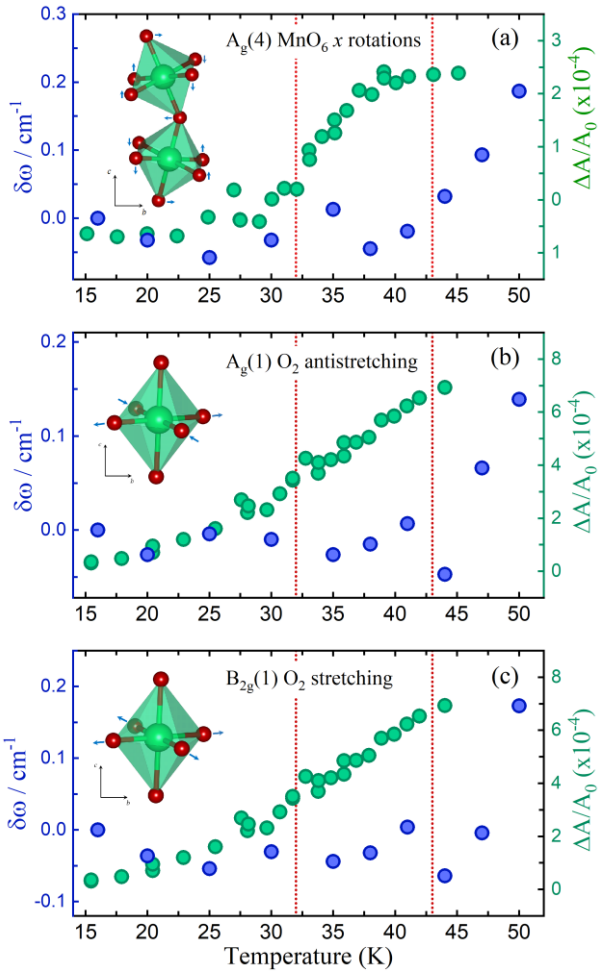

Figure 5. Comparison of the temperature-dependence of the phonon energy ($\delta\omega(T) = \omega(16K) - \omega(T)$) and the lattice planes corresponding to (a) $A_g(4)$ ($A = b \times c$), (b) $A_g(1)$ and (c) $B_{2g}(1)$ ($A = a \times b$). The lattice parameters were obtained from Ref. (Pomjakushin et al., 2009).

Figure 5 shows the frequency change relative to the lower measured temperature ($\delta\omega(T) = \omega(16K) - \omega(T)$) for the $A_g(4)$, $A_g(1)$ and $B_{2g}(1)$ modes of *o*-TMO (green circles) compared to the variation of $A = b \times c$ (Figure 5 (a)) and $A = a \times c$ planes (Figure 5 (b) and (c)) calculated from the data reported by Pomjakushin et al. (Pomjakushin et al., 2009). As can be seen, there is no correlation between all three coupled phonons with their respective expansion planes in the temperature range of the lattice distortions induced by the magneto-structural coupling. These results also support the spin-phonon origin of the frequency renormalization.

Similarly to o-TMO, other members of the *o*-RMO_3 family also showed a spin-phonon coupling starting around the temperatures at which the magnetically ordered phase arises (Laverdière et al., 2006; Mansouri et al., 2017). However, unlike other *o*-RMO_3 compounds, the o-TMO phonons presented a hardening effect on phonon positions

instead of a softening, as observed by Laverdière et al. (Laverdière et al., 2006) Also, the magnitude of the phonon renormalization due to spin-phonon coupling in o-TMO is weaker in comparison to those observed for $PrMnO_3$ (Laverdière et al., 2006) and $ErMnO_3$ (Vermette et al., 2008), but still comparable to the one of the $A_g(1)$ phonon of $DyMnO_3$ (Laverdière et al., 2006). In contrast to our observations, previous reports claim that the spin-phonon coupling is negligible in compounds with small r_R and incommensurate AFM ordering. Conversely, the phonon wavenumber and FWHM *o*-TMO indicate a weak, but not negligible, spin-phonon coupling rising nearby the temperature of the incommensurate AFM ordering.

The renormalization effects experienced by the *o*-TMO phonons can be observed slightly above T_N. Laverdière et al. (Laverdière et al., 2006) highlighted this as a common effect also found in other compounds as $LaMnO_3$ (Granado et al., 1999) $PrMnO_3$, $NdMnO_3$, $SmMnO_3$ and $DyMnO_3$ (Laverdière et al., 2006), in which the spin-phonon coupling also starts well above (around 30 K) the magnetic ordering temperature. In such cases, the authors suggest that the renormalization above T_N could be explained by in-phase ferromagnetic interactions existing even in paramagnetic phases (Laverdière et al., 2006).

The renormalization effect of a phonon frequency ($\Delta\omega$) due to spin-phonon coupling can be modeled by taking into account the static spin-spin correlation average function (Baltensperger & Helman, 1968; Lockwood & Cottam, 1988) as proposed by Granado et al. (Granado et al., 1999), which leads to the following relation

$$\Delta\omega \equiv \omega - \omega_0 = \frac{2}{m\omega} \sum_{i,j>i} \frac{\partial^2 J_{ij}}{\partial u^2} \langle S_i \cdot S_j \rangle \tag{3}$$

where ω is the renormalized phonon frequency due to the spin-phonon coupling, ω_0 is the phonon frequency in the absence of a coupling effect, m is the oxygen mass, u is the atomic displacement during the vibrational motion, J_{ij} is the exchange integral between the i^{th} and the j^{th}magnetic ion and $\langle S_i \cdot S_j \rangle$ denotes the statistical-mechanical average for adjacent spins moments. Thus, in the paramagnetic phase, there are no ordered spin moments and the term $\langle S_i \cdot S_j \rangle$ vanishes, whereas in a magnetically ordered phase, an additional contribution to phonon frequency is expected due to the coupling effect. It is convenient to determine the magnetic contribution due to phonon renormalization by

using the mean-field approach as $(\langle S^z \rangle / S)^2$ (Prosnikov et al., 2018), where $\langle S^z \rangle$ is obtained from the Brillouin function giving the relation:

$$\langle S_i \cdot S_j \rangle = \left(\frac{M(T)}{M_0} \right)^2 \quad (4)$$

The term outside of brackets on the right side of equation (3) is commonly called the λ factor or coupling constant (Araújo et al., 2018; Aytan et al., 2017; El Amrani et al., 2014; Ferreira et al., 2009; Lockwood & Cottam, 1988; Mahana et al., 2017; Silva Júnior & Paschoal, 2014; Sushkov et al., 2005). There is a systematic trend on phonon frequency renormalization inferred from a considerable number of materials in which the spin-phonon coupling was confirmed. Thus, in the magnetically ordered phases, ferromagnetic materials usually present a softening of the phonon frequencies (Iliev et al., 2007; Macedo Filho et al., 2013; Rosivaldo X. Silva et al., 2017), while in antiferromagnetic materials, a hardening effect is observed (Srinu Bhadram et al., 2013; Vermette et al., 2008). However, the coupling constant has a complex dependence on the magnetic order and the phonon atomic displacements, making it a complicated factor. In this way, several compounds not following the general behavior have been reported in recent years (Aytan et al., 2017; El Amrani et al., 2014; Laverdière et al., 2006; Mahana et al., 2017; R. X. Silva et al., 2013). In the case of o-$TmMnO_3$, we observe a hardening in the phonon frequencies due to the spin-phonon coupling, which is consistent with antiferromagnetic phases previously reported in the literature (Pomjakushin et al., 2009; Shimamoto et al., 2017; Tachibana et al., 2007).

As mentioned before, Granado et al. (Granado et al., 1999) proposed a mechanism to modulate the spin-phonon coupling effect in a stretching mode of $LaMnO_3$ by using the mean-field theory approach:

$$\Delta\omega_{s-ph} \approx \frac{2}{m\omega} \frac{\partial^2 J_1}{\partial u^2} \left(\frac{M_{sublatt}(T)}{4\mu_B} \right)^2 \quad (5)$$

This model has been employed to describe the spin-phonon coupling in several perovskites as $Gd(Co_{1/2}Mn_{1/2})O_3$ (R. X. Silva et al., 2013), Y_2NiMnO_6 (Macedo Filho et al., 2013), and $BiCrO_3$ (Araújo et al., 2020), as well as, in non-perovskite compounds like NiO (Aytan et al., 2017) and Cu_2OCl_2 (Araújo et al., 2018). However, in the case of incommensurate magnetic ordering, an extension of this model becomes necessary. Kimura et al. (Kimura, Ishihara, et al., 2003), considering the inclusion of the nearest-neighbor (NN) and the next-nearest-neighbor (NNN) interactions, have rewritten the phonon renormalization as:

$$\Delta\omega = \frac{1}{2m\omega}\sum_{r}\frac{\partial^2 J(\boldsymbol{r})}{\partial u^2}\langle \boldsymbol{S}_i \cdot \boldsymbol{S}_{i+r}\rangle \quad (6)$$

For an incommensurate ordering with propagation vector $\boldsymbol{k}$, Laverdière et al. (Laverdière et al., 2006) proposed the following spin correlation function

$$\langle \boldsymbol{S}_i \cdot \boldsymbol{S}_{i+r}\rangle = K(T)\cos(2\pi \boldsymbol{k}\cdot \boldsymbol{r}) \quad (7)$$

where $K(T)$ is a temperature-dependent prefactor $[K(T) \propto M^2_{sublatt}(T)]$.

Pomjakushin et al. (Pomjakushin et al., 2009) showed that the first magnetic transition of *o*-TMO drives the paramagnetic phase into an incommensurate AFM phase at 42K. The incommensurate phase has $\boldsymbol{k} = (k_x, 0,0)$, with k_x varying from 0.45 to 0.5, when the incommensurate AFM structure becomes an E-type AFM structure. Mn^{3+} ions can be classified according the o-TMO magnetic structure as follows, NN: four ions (J_1) placed at $\boldsymbol{r} = \pm 0.5x \pm 0.5z$ and NNN: two ions (J_2) at $\boldsymbol{r} = \pm x$ and two ions (J_3) at $\boldsymbol{r} = \pm z$. Thus, the resulting phonon renormalization is given by (Laverdière et al., 2006) ($D_i = \partial^2 J_i/\partial u^2$):

$$\Delta\omega = \frac{K(T)}{m\omega}[2D_1\cos(\pi k_x) + D_2\cos(2\pi k_x) + D_3] \quad (8)$$

In the case of E-type magnetic phase of o-TMO with $k_x = 0.5$, the NN contributions cancel themselves since each Mn^{3+} ion is surrounded by two sets of ions with opposite spin moments (Laverdière et al., 2006; Pomjakushin et al., 2009) and equation (8) becomes:

$$\Delta\omega = \frac{2}{m\omega}[D_3 - D_2]\left(\frac{M(T)}{M_0}\right)^2 \quad (9)$$

Based on these considerations, in both magnetically ordered phases of *o*-TMO, the phonon renormalization should be proportional to $(M(T)/M_0)^2$. Thus, in Figure 6, the $\Delta\omega$ for the selected phonons ($A_g(4)$, $A_g(1)$ and $B_{2g}(1)$) is plotted as a function of $(M(T)/M_0)^2$. As it was discussed previously, a non-zero $\Delta\omega$ is observed just above T_N (~50K), which is characterized by the rising of the phonon renormalization without an apparent linear trend. In fact, a proportionality constant cannot be expected in this region since $\Delta\omega$ not only depends on $(M(T)/M_0)^2$ but also on the k_x value of the incommensurate phase (eq. (8)). A linear dependence is observed below ~35 K. This temperature agrees quite well with the lock-in phase transition into the E-type AFM phase, where eq. (9) should describe the $\Delta\omega$ behavior. By fitting AFM region with a linear function, the slope obtained for $B_{2g}(1)$, $A_g(1)$ and $A_g(4)$ phonons were $-0.2(5)$, $-0.1(2)$,

and $-0.2(3)$ cm^{-1}, respectively. These very small values suggest that $\Delta\omega$ as a function of $(M(T)/M_0)^2$ becomes approximately constant, implying that the factor $[D_3 - D_2]$ in eq. (9) should be neglectable in the E-type AFM phase, in good accordance with the Laverdière *et al.* observations (Laverdière et al., 2006).

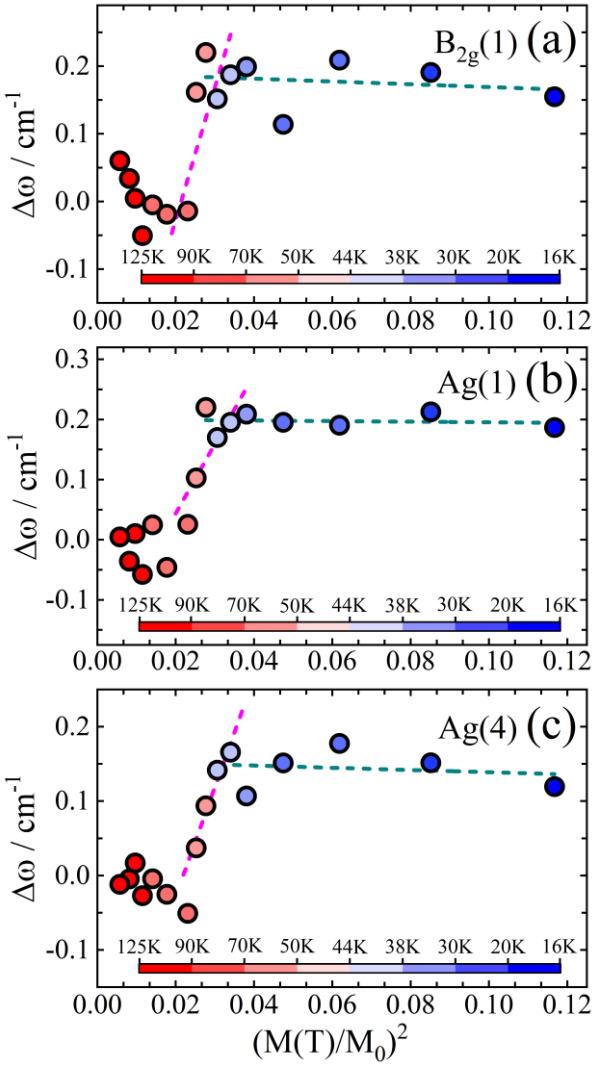

Figure 6. Panels a-c: Temperature dependence of the departure from anharmonic behavior of selected phonons as a function of $(M(T)/M_0)^2$, the pink and dark green dashed lines are the linear fit of data in the IC and E-type AFM phases, respectively.

The neglectable spin-phonon coupling in the E-type AFM phase is evidenced in Figure 4 since the phonon wavenumber follows Balkanski's model but slightly shifted towards higher values. A similar phenomenon also can be observed in the 384 cm^{-1} mode of $TbMnO_3$ and the 516.5 and 494 cm^{-1} modes of $DyMnO_3$ (Mansouri et al., 2017). In both cases, the renormalization of phonon frequencies starts around the temperatures in which an incommensurate magnetic structure rises (Harikrishnan et al., 2009; Kenzelmann et al., 2005; Prokhnenko et al., 2007), and, after the second magnetic transition, the renormalization process becomes constant. In such cases, the saturation in

the phonon frequency renormalization suggests that the spin-phonon coupling is not the only factor involved in the temperature dependence of the phonon wavenumbers.

Aiming to investigate such effects, Xu et al. (Xu et al., 2007) developed a theoretical model taking into account possible contributions of the orbital ordering to the spin-phonon coupling. Considering this contribution, the frequency shift $\Delta\omega_{OSP}(T)$ can be rewritten as a function of the effective spin-phonon coupling (J_{ij}^{s-ph}) and the effective orbital-spin-phonon coupling (J_{ij}^{oo}):

$$\Delta\omega_{OSP}(T) \approx \frac{2}{m\omega}\sum_{i,j>i}\left(\frac{\partial^2 J_{ij}^{s-ph}}{\partial u^2}\, S_iS_j + 4\frac{\partial^2 J_{ij}^{oo}}{\partial u^2} S_jS_j\tau_i\tau_j\right) \qquad (10)$$

where $\tau_i\tau_j$ is the orbital correlation operator for the i and j Mn^{3+} ions. By using a multivariate Taylor expansion $\sum_{i,j}\left(S_iS_j\tau_i\tau_j\right) \approx \sum_{i,j}\left(\langle S_iS_j\rangle\langle\tau_i\tau_j\rangle + \langle S_iS_j\rangle\delta\tau + \langle\tau_i\tau_j\rangle\delta S\right)$, where $\delta\tau \equiv \tau_i\tau_j - \langle\tau_i\tau_j\rangle|_{S_iS_j=\langle S_iS_j\rangle}$ and $\delta S \equiv S_iS_j - \langle S_iS\rangle|_{\tau_i\tau_j=\langle\tau_i\tau_j\rangle}$, it is possible to establish an expression for the frequency shift due to the combined couplings (Mansouri et al., 2017; Xu et al., 2007).

$$\Delta\omega_{OSP}(T) \approx \frac{2}{m\omega}\sum_{i,j>i}\left[\left(\frac{\partial^2 J_{ij}^{s-ph}}{\partial u^2} + 4\frac{\partial^2 J_{ij}^{oo}}{\partial u^2}\left(\langle\tau_i\tau_j\rangle + \delta S\right)\right)\langle S_iS_j\rangle + 4\frac{\partial^2 J_{ij}^{oo}}{\partial u^2}\langle\tau_i\tau_j\rangle\delta S\right] \qquad (11)$$

This model was previously applied to describe the spin-phonon coupling of A-type AFM materials (Mansouri et al., 2017; Xu et al., 2007). However, it needs to be modified in the case of the incommensurate to E-type magnetic transition based on eq. (8) (Laverdière et al., 2006). Thus, for an incommensurate magnetic order, the $\Delta\omega(T)$ renormalization of coupled phonon modes can be rewritten as:

$$\Delta\omega_{OSP}(T) \approx \frac{2}{m\omega}\left[\left(2\left(D_1 + D_1^{oo}\right)\cos(\pi k_x) + \left(D_2 + D_2^{oo}\right)\cos(2\pi k_x) + \left(D_3 + D_3^{oo}\right)\right)K(T) + D'_4\right] \qquad (12)$$

where $D_i^{oo} = 4\left(\langle\tau_i\tau_j\rangle + \delta S\right)\partial^2 J_{ij}^{oo}/\partial u^2$ and $D'_4 = 4\delta S\sum\langle\tau_i\tau_j\rangle\,\partial^2 J_{ij}^{oo}/\partial u^2$. This result does not change the previous discussion about the spin-phonon coupling in the

incommensurate phase because of the complex dependence on k_x. However, in the E-type AFM phase ($k_x = 0.5$) eq. (12) is reduced to

$$\Delta\omega_{OSP}(T) \approx \frac{2}{m\omega}\left[\left(D_3 - D_2 + D_3^{oo} - D_2^{oo}\right)\left(\frac{M(T)}{M_0}\right)^2 + 4D'_4\right] \quad (13)$$

The last equation has a linear dependence on the square of sublattice magnetization, where the intercept is related to the effective orbital-spin-phonon coupling (k_{OSP}) and should be non-zero only in cases where this interaction exists. Previous reports have proposed that $D_3 \cong D_2$ in the E-type AFM phase based on the observation of a neglectable spin-phonon coupling (Laverdière et al., 2006). However, the observed null slope also requires the same condition for the contribution of the orbital-spin-phonon coupling ($D_3^{oo} \cong D_2^{oo}$). On the other hand, the three phonons shown in Figure 6 have a finite intercept of $0.19(3), 0.20(1), \text{and } 0.16(3)$ cm^{-1} for $B_{2g}(1)$, $A_g(1)$, and $A_g(4)$, respectively. These values are similar but smaller than those reported by Mansouri et al. (Mansouri et al., 2017), agreeing with the proposal that k_{OSP} value decreases with the ionic radius of the rare-earth in the *o*-RMO family.

4. Conclusions

The spin-phonon coupling in bulk *o*-TMO was explored by low-temperature Raman spectroscopy measurements. Our results revealed that below 48 K, the $A_g(4)$, $A_g(3)$ and $B_{2g}(1)$ phonons temperature dependence depart from the model based on the anharmonicity exhibiting renormalization effects on the frequency and FWHM parameters. This feature coincides with the paramagnetic to incommensurate AFM phase transition showing a well-defined spin-phonon coupling in contradiction to previous assumptions. The $\Delta\omega$ vs $(M(T)/M_0)^2$ dependence reveals a complex behavior in the incommensurate phase. However, approximately at the lock-in transition into the E-type magnetic structure, the frequency shift becomes constant. Based on previous studies a model was proposed where the phonon renormalization has a contribution from an orbital-spin-phonon coupling, which becomes the dominant effect in the E-type AFM phase. The low magnitude of phonon frequency renormalization indicates the spin-phonon coupling on *o*-$TmMnO_3$ is weaker than those reported for its hexagonal phase and other *o*-RMO compounds, but is still comparable with those elsewhere in the o-RMO family, as $DyMnO_3$.

5. References

Araújo, B. S., Arévalo-López, A. M., Attfield, J. P., Paschoal, C. W. A., & Ayala, A. P. (2018). Spin-phonon coupling in melanothallite Cu2OCl 2. *Applied Physics Letters*, *113*(22), 222901. https://doi.org/10.1063/1.5054928

Araújo, B. S., Arévalo-López, A. M., Santos, C. C., Attfield, J. P., Paschoal, C. W. A., & Ayala, A. P. (2020). Spin–phonon coupling in monoclinic BiCrO3. *Journal of Applied Physics*, *127*(11), 114102. https://doi.org/10.1063/1.5143347

Aytan, E., Debnath, B., Kargar, F., Barlas, Y., Lacerda, M. M., Li, J. X., Lake, R. K., Shi, J., & Balandin, A. A. (2017). Spin-phonon coupling in antiferromagnetic nickel oxide. *Applied Physics Letters*, *111*(25), 252402. https://doi.org/10.1063/1.5009598

Baldini, E., Kubacka, T., Mallett, B. P. P., Ma, C., Koohpayeh, S. M., Zhu, Y., Bernhard, C., Johnson, S. L., & Carbone, F. (2018). Lattice-mediated magnetic order melting in TbMnO3. *Physical Review B*, *97*(12), 125149. https://doi.org/10.1103/PhysRevB.97.125149

Balkanski, M., Wallis, R. F. R., & Haro, E. (1983). Anharmonic effects in light scattering due to optical phonons in silicon. *Physical Review B*, *28*(4), 1928–1934. https://doi.org/10.1103/PhysRevB.28.1928

Baltensperger, W., & Helman, J. S. J. (1968). Influence of magnetic order in insulators on the optical phonon frequency. *Helvetica Physica Acta*, *41*(6–7), 668. https://doi.org/10.5169/seals-113910

Basistyy, R., Stanislavchuk, T. N., Sirenko, A. A., Litvinchuk, A. P., Kotelyanskii, M., Carr, G. L., Lee, N., Wang, X., & Cheong, S. W. (2014). Infrared-active optical phonons and magnetic excitations in the hexagonal manganites RMn O3 (R=Ho, Er, Tm, Yb, and Lu). *Physical Review B - Condensed Matter and Materials Physics*, *90*(2), 1–12. https://doi.org/10.1103/PhysRevB.90.024307

Bauman, R. P., Rousseau, D. L., Porto, S. P. S., Bauman, R. P., Porto, S. P. S., Rousseau, D. L., & Porto, S. P. S. (1981). Normal mode determination in crystals. *Journal of Raman Spectroscopy*, *10*(1), 253–290. https://doi.org/10.1002/jrs.1250100152

de Andrés, A., Martínez, J. L., Alonso, J. M., Herrero, E., Prieto, C., Alonso, J. A., Agulló, F., & García-Hernández, M. (1999). Raman phonons in orthorhombic manganites. *Journal of Magnetism and Magnetic Materials*, *196–197*, 453–454. https://doi.org/10.1016/S0304-8853(98)00810-5

Eiter, H.-M., Jaschke, P., Hackl, R., Bauer, A., Gangl, M., & Pfleiderer, C. (2014). Raman

study of the temperature and magnetic-field dependence of the electronic and lattice properties of MnSi. *Physical Review B*, *90*(2), 024411. https://doi.org/10.1103/PhysRevB.90.024411

El Amrani, M., Zaghrioui, M., Ta Phuoc, V., Gervais, F., & Massa, N. E. (2014). Local symmetry breaking and spin–phonon coupling in SmCrO3 orthochromite. *Journal of Magnetism and Magnetic Materials*, *361*, 1–6. https://doi.org/10.1016/j.jmmm.2014.02.057

Ferreira, W. S., Agostinho Moreira, J., Almeida, A., Chaves, M. R., Araújo, J. P., Oliveira, J. B., MacHado Da Silva, J. M., Sá, M. A., Mendonça, T. M., Simeão Carvalho, P., Kreisel, J., Ribeiro, J. L., Vieira, L. G., Tavares, P. B., & Mendonça, S. (2009). Spin-phonon coupling and magnetoelectric properties: EuMnO3 versus GdMnO3. *Physical Review B - Condensed Matter and Materials Physics*, *79*(5), 1–10. https://doi.org/10.1103/PhysRevB.79.054303

Garganourakis, M., Bodenthin, Y., De Souza, R. A., Scagnoli, V., Dönni, A., Tachibana, M., Kitazawa, H., Takayama-Muromachi, E., & Staub, U. (2012). Magnetic and electronic orderings in orthorhombic RMnO3 (R=Tm, Lu) studied by resonant soft x-ray powder diffraction. *Physical Review B - Condensed Matter and Materials Physics*, *86*(5), 1–5. https://doi.org/10.1103/PhysRevB.86.054425

Goto, T., Kimura, T., Lawes, G., Ramirez, A. P., & Tokura, Y. (2004). Ferroelectricity and Giant Magnetocapacitance in Perovskite Rare-Earth Manganites. *Physical Review Letters*, *92*(25), 257201. https://doi.org/10.1103/PhysRevLett.92.257201

Granado, E., García, A., Sanjurjo, J. A., Rettori, C., Torriani, I., Prado, F., Sánchez, R. D., Caneiro, A., & Oseroff, S. B. (1999). Magnetic ordering effects in the Raman spectra of La1-xMn1-xO3. *Physical Review B*, *60*(17), 11879–11882. https://doi.org/10.1103/PhysRevB.60.11879

Han, T. C., & Chao, H. H. (2010). Observation of large electric polarization in orthorhombic TmMnO3 thin films. *Applied Physics Letters*, *97*(23), 232902. https://doi.org/10.1063/1.3524500

Harikrishnan, S., Rößler, S., Naveen Kumar, C. M., Bhat, H. L., Rößler, U. K., Wirth, S., Steglich, F., & Elizabeth, S. (2009). Phase transitions and rare-earth magnetism in hexagonal and orthorhombic DyMnO3 single crystals. *Journal of Physics: Condensed Matter*, *21*(9), 096002. https://doi.org/10.1088/0953-8984/21/9/096002

Hwang, H. Y., Cheong, S.-W., Radaelli, P. G., Marezio, M., & Batlogg, B. (1995). Lattice Effects on the Magnetoresistance in Doped LaMnMnO3. *Physical Review Letters*,

75(5), 914–917. https://doi.org/10.1103/PhysRevLett.75.914

Iliev, M. N., Abrashev, M. V., Laverdière, J., Jandl, S., Gospodinov, M. M., Wang, Y.-Q., & Sun, Y.-Y. (2006). Distortion-dependent Raman spectra and mode mixing in RMnO3 perovskites (R=La,Pr,Nd,Sm,Eu,Gd,Tb,Dy,Ho,Y). *Physical Review B*, *73*(6), 064302. https://doi.org/10.1103/PhysRevB.73.064302

Iliev, M. N., Abrashev, M. V., Litvinchuk, A. P., Hadjiev, V. G., Guo, H., & Gupta, A. (2007). Raman spectroscopy of ordered double perovskite La2CoMnO6. *Physical Review B*, *75*(10), 104118. https://doi.org/10.1103/PhysRevB.75.104118

Kenzelmann, M., Harris, A. B., Jonas, S., Broholm, C., Schefer, J., Kim, S. B., Zhang, C. L., Cheong, S.-W., Vajk, O. P., & Lynn, J. W. (2005). Magnetic Inversion Symmetry Breaking and Ferroelectricity in TbMnO3. *Physical Review Letters*, *95*(8), 087206. https://doi.org/10.1103/PhysRevLett.95.087206

Kimura, T., Goto, T., Shintani, H., Ishizaka, K., Arima, T., & Tokura, Y. (2003). Magnetic control of ferroelectric polarization. *Nature*, *426*(6962), 55–58. http://dx.doi.org/10.1038/nature02018

Kimura, T., Ishihara, S., Shintani, H., Arima, T., Takahashi, T., Ishizaka, K., & Tokura, Y. (2003). Distorted perovskite with eg1 configuration as a frustrated spin system. *Physical Review B - Condensed Matter and Materials Physics*, *68*(6), 3–6. https://doi.org/10.1103/PhysRevB.68.060403

Laverdière, J., Jandl, S., Mukhin, A. A., Ivanov, V. Y., Ivanov, V. G., & Iliev, M. N. (2006). Spin-phonon coupling in orthorhombic RMO3 (R=Pr,Nd,Sm,Eu,Gd,Tb,Dy,Ho,Y): A Raman study. *Physical Review B*, *73*(21), 214301. https://doi.org/10.1103/PhysRevB.73.214301

Lockwood, D. J., & Cottam, M. G. (1988). The spin - phonon interaction in FeF2 and MnF2 studied by Raman spectroscopy. *J. Appl. Phys.*, *64*(1988), 5876.

Macedo Filho, R. B., Pedro Ayala, A., & William de Araujo Paschoal, C. (2013). Spin-phonon coupling in Y2NiMnO6 double perovskite probed by Raman spectroscopy. *Applied Physics Letters*, *102*(19), 192902. https://doi.org/10.1063/1.4804988

Mahana, S., Rakshit, B., Basu, R., Dhara, S., Joseph, B., Manju, U., Mahanti, S. D., & Topwal, D. (2017). Local inversion symmetry breaking and spin-phonon coupling in the perovskite GdCrO3. *Physical Review B*, *96*(10), 104106. https://doi.org/10.1103/PhysRevB.96.104106

Mansouri, S., Jandl, S., Mukhin, A., Ivanov, V. Y., & Balbashov, A. (2017). A comparative Raman study between PrMnO 3, NdMnO 3, TbMnO 3 and DyMnO 3.

Scientific Reports, *7*(1), 13796. https://doi.org/10.1038/s41598-017-12714-8

Martín-Carrón, L., De Andrés, A., Martínez-Lope, M. J., Casais, M. T., & Alonso, J. A. (2001). Raman phonons and light scattering in RMnO3(R=La, Pr, Nd, Ho, Er Tb and Y) orthorhombic and hexagonal manganites. *Journal of Alloys and Compounds*, *323–324*, 494–497. https://doi.org/10.1016/S0925-8388(01)01047-7

Martín-Carrón, L., De Andrés, A., Martínez-Lope, M. J., Casais, M. T., & Alonso, J. A. (2002). Raman phonons as a probe of disorder, fluctuations, and local structure in doped and undoped orthorhombic and rhombohedral manganites. *Physical Review B - Condensed Matter and Materials Physics*, *66*(17), 1–8. https://doi.org/10.1103/PhysRevB.66.174303

Massa, N. E., del Campo, L., Meneses, D. D. S., Echegut, P., Martínez-Lope, M. J., & Alonso, J. A. (2014). Phonons and hybrid modes in the high and low temperature far infrared dynamics of hexagonal TmMnO 3. *Journal of Physics: Condensed Matter*, *26*(27), 275901. https://doi.org/10.1088/0953-8984/26/27/275901

Mukherjee, S., Dönni, A., Nakajima, T., Mitsuda, S., Tachibana, M., Kitazawa, H., Pomjakushin, V., Keller, L., Niedermayer, C., Scaramucci, A., & Kenzelmann, M. (2017). E-type noncollinear magnetic ordering in multiferroic o−LuMnO3. *Physical Review B*, *95*(10), 104412. https://doi.org/10.1103/PhysRevB.95.104412

Niitaka, S., Azuma, M., Takano, M., Nishibori, E., Takata, M., & Sakata, M. (2004). Crystal structure and dielectric and magnetic properties of BiCrO 3 as a ferroelectromagnet. *Solid State Ionics*, *172*(1-4 SPEC. ISS.), 557–559. https://doi.org/10.1016/j.ssi.2004.01.060

Pomjakushin, V. Y., Kenzelmann, M., Dönni, A., Harris, A. B., Nakajima, T., Mitsuda, S., Tachibana, M., Keller, L., Mesot, J., Kitazawa, H., & Takayama-Muromachi, E. (2009). Evidence for large electric polarization from collinear magnetism in TmMnO3. *New Journal of Physics*, *11*(4), 043019. https://doi.org/10.1088/1367-2630/11/4/043019

Prokhnenko, O., Feyerherm, R., Dudzik, E., Landsgesell, S., Aliouane, N., Chapon, L. C., & Argyriou, D. N. (2007). Enhanced Ferroelectric Polarization by Induced Dy Spin Order in Multiferroic DyMnO3. *Physical Review Letters*, *98*(5), 057206. https://doi.org/10.1103/PhysRevLett.98.057206

Prosnikov, M. A., Smirnov, A. N., Davydov, V. Y., Pisarev, R. V., Lyubochko, N. A., & Barilo, S. N. (2018). Magnetic dynamics and spin-phonon coupling in the antiferromagnet Ni 2 NbBO 6. *Physical Review B*, *98*(10), 104404.

https://doi.org/10.1103/PhysRevB.98.104404

Salama, H. A., Stewart, G. A., Hutchison, W. D., Nishimura, K., Scott, D. R., & O'Neill, H. S. (2010). A 169Tm-Mössbauer spectroscopy investigation of orthorhombic phase. *Solid State Communications*, *150*(5–6), 289–291. https://doi.org/10.1016/j.ssc.2009.11.002

Shimamoto, K., Mukherjee, S., Bingham, N. S., Suszka, A. K., Lippert, T., Niedermayer, C., & Schneider, C. W. (2017). Single-axis-dependent structural and multiferroic properties of orthorhombic RMn O3(R=Gd-Lu). *Physical Review B*, *95*(18), 1–9. https://doi.org/10.1103/PhysRevB.95.184105

Silva Júnior, F. M., & Paschoal, C. W. A. (2014). Spin-phonon coupling in BaFe 12 O 19 M-type hexaferrite. *Journal of Applied Physics*, *116*(24), 244110. https://doi.org/10.1063/1.4904062

Silva, R. X., Reichlova, H., Marti, X., Barbosa, D. A. B., Lufaso, M. W., Araujo, B. S., Ayala, A. P., & Paschoal, C. W. A. (2013). Spin-phonon coupling in Gd(Co 1/2 Mn 1/2)O 3 perovskite. *Journal of Applied Physics*, *114*(19), 194102. https://doi.org/10.1063/1.4829902

Silva, Rosivaldo X., Castro Júnior, M. C., Yáñez-Vilar, S., Andújar, M. S., Mira, J., Señarís-Rodríguez, M. A., & Paschoal, C. W. A. (2017). Spin-phonon coupling in multiferroic Y2CoMnO6. *Journal of Alloys and Compounds*, *690*, 909–915. https://doi.org/10.1016/j.jallcom.2016.07.010

Spaldin, N. A., & Ramesh, R. (2019). Advances in magnetoelectric multiferroics. *Nature Materials*, *18*(3), 203–212. https://doi.org/10.1038/s41563-018-0275-2

Srinu Bhadram, V., Rajeswaran, B., Sundaresan, A., & Narayana, C. (2013). Spin-phonon coupling in multiferroic RCrO3 (R-Y, Lu, Gd, Eu, Sm): A Raman study. *EPL (Europhysics Letters)*, *101*(1), 17008. https://doi.org/10.1209/0295-5075/101/17008

Sugawara, F., Iida, S., Syono, Y., & Akimoto, S. (1965). New Magnetic Perovskites BiMnO3 and BiCrO3. *Journal of the Physical Society of Japan*, *20*(8), 1529–1529. https://doi.org/10.1143/JPSJ.20.1529

Sugawara, F., Iiida, S., Syono, Y., & Akimoto, S. (1968). Magnetic Properties and Crystal Distortions of BiMnO 3 and BiCrO 3. *Journal of the Physical Society of Japan*, *25*(6), 1553–1558. https://doi.org/10.1143/JPSJ.25.1553

Sushkov, A. B., Tchernyshyov, O., II, W. R., Cheong, S. W., & Drew, H. D. (2005). Probing Spin Correlations with Phonons in the Strongly Frustrated Magnet ZnCr2O4. *Physical Review Letters*, *94*(13), 137202.

https://doi.org/10.1103/PhysRevLett.94.137202

Tachibana, M., Shimoyama, T., Kawaji, H., Atake, T., & Takayama-Muromachi, E. (2007). Jahn-Teller distortion and magnetic transitions in perovskite RMn O3 (R=Ho, Er, Tm, Yb, and Lu). *Physical Review B - Condensed Matter and Materials Physics*, *75*(14), 2–6. https://doi.org/10.1103/PhysRevB.75.144425

Uusi-Esko, K., Malm, J., Imamura, N., Yamauchi, H., & Karppinen, M. (2008). Characterization of RMnO3 (R=Sc, Y, Dy-Lu): High-pressure synthesized metastable perovskites and their hexagonal precursor phases. *Materials Chemistry and Physics*, *112*(3), 1029–1034. https://doi.org/10.1016/j.matchemphys.2008.07.009

Vermette, J., Jandl, S., & Gospodinov, M. M. (2008). Raman study of spin–phonon coupling in ErMnO 3. *Journal of Physics: Condensed Matter*, *20*(42), 425219. https://doi.org/10.1088/0953-8984/20/42/425219

Wang, L. J., Feng, S. M., Zhu, J. L., Yu, R. C., Jin, C. Q., Yu, W., Wang, X. H., & Li, L. T. (2007). Ferroelectricity of multiferroic hexagonal TmMn O3 ceramics synthesized under high pressure. *Applied Physics Letters*, *91*(17), 4–7. https://doi.org/10.1063/1.2800816

Windsor, Y. W., Ramakrishnan, M., Rettig, L., Alberca, A., Bothschafter, E. M., Staub, U., Shimamoto, K., Hu, Y., Lippert, T., & Schneider, C. W. (2015). Interplay between magnetic order at Mn and Tm sites alongside the structural distortion in multiferroic films of o−TmMnO3. *Physical Review B*, *91*(23), 235144. https://doi.org/10.1103/PhysRevB.91.235144

Wojdyr, M. (2010). Fityk : a general-purpose peak fitting program. *Journal of Applied Crystallography*, *43*(5), 1126–1128. https://doi.org/10.1107/S0021889810030499

Xu, J., Park, J. H., & Jang, H. M. (2007). Orbital-spin-phonon coupling in Jahn-Teller-distorted LaMnO3: Softening of the 490 and 610 cm-1 Raman-active modes. *Physical Review B - Condensed Matter and Materials Physics*, *75*(1), 10–13. https://doi.org/10.1103/PhysRevB.75.012409

Yen, F., dela Cruz, C., Lorenz, B., Galstyan, E., Sun, Y. Y., Gospodinov, M., & Chu, C. W. (2007). Magnetic phase diagrams of multiferroic hexagonal RMnO3 (R = Er, Yb, Tm, and Ho). *Journal of Materials Research*, *22*(08), 2163–2173. https://doi.org/10.1557/jmr.2007.0271

Zhou, J.-S., Goodenough, J. B., Gallardo-Amores, J. M., Morán, E., Alario-Franco, M. A., & Caudillo, R. (2006). Hexagonal versus perovskite phase of manganite (R=Y,

Ho, Er, Tm, Yb, Lu). *Physical Review B*, *74*(1), 014422. https://doi.org/10.1103/PhysRevB.74.014422